



Automated crop plant detection based on the fusion of color and depth images for robotic weed control

Jingyao Gai | Lie Tang | Brian L. Steward

Agricultural and Biosystems Engineering, Iowa State University, Ames, Iowa

Correspondence

Lie Tang, Agricultural and Biosystems Engineering, Iowa State University, Ames, IA, 50011.
Email: lietang@iastate.edu

Funding information

National Institute of Food and Agriculture, Grant/Award Number: 20136702121126; Leopold Center for Sustainable Agriculture, Grant/Award Numbers: M2009-23, M2012-24

Abstract

Robotic weeding enables weed control near or within crop rows automatically, precisely and effectively. A computer-vision system was developed for detecting crop plants at different growth stages for robotic weed control. Fusion of color images and depth images was investigated as a means of enhancing the detection accuracy of crop plants under conditions of high weed population. In-field images of broccoli and lettuce were acquired 3–27 days after transplanting with a Kinect v2 sensor. The image processing pipeline included data preprocessing, vegetation pixel segmentation, plant extraction, feature extraction, feature-based localization refinement, and crop plant classification. For the detection of broccoli and lettuce, the color-depth fusion algorithm produced high true-positive detection rates (91.7% and 90.8%, respectively) and low average false discovery rates (1.1% and 4.0%, respectively). Mean absolute localization errors of the crop plant stems were 26.8 and 7.4 mm for broccoli and lettuce, respectively. The fusion of color and depth was proved beneficial to the segmentation of crop plants from background, which improved the average segmentation success rates from 87.2% (depth-based) and 76.4% (color-based) to 96.6% for broccoli, and from 74.2% (depth-based) and 81.2% (color-based) to 92.4% for lettuce, respectively. The fusion-based algorithm had reduced performance in detecting crop plants at early growth stages.

KEY WORDS

computer vision, crop detection, robotic weeding, sensor fusion

1 | INTRODUCTION

Recently, with evolving consumer tastes, the interest in vegetables, especially natural, organic vegetables has grown (USDA, 2016, 2017). Compared with conventional farmers who control weeds using synthetic herbicides, organic farmers are mostly limited to non-chemical weed control strategies, of which mechanical weeding methods such as hand-weeding, tillage, and cultivation are common.

Mechanical weed control can be classified into two categories based on the target area of control relative to the crop row (Pannacci, Lattanzi, & Tei, 2017): (a) interrow weeding (between crop rows), and (b) intrarow weeding (within or close to crop rows). Weeds between crop rows are relatively easy to control by mechanical

cultivation. Intrarow weed control, however, is challenging because of the high risk of damaging crop plants when controlling weed plants close to the crop plants. Hand-weeding is commonly used, but it is laborious and costly. Although mechanical intrarow weeding machines are available, such as finger weeder and torsion weeder (Van Der Weide et al., 2008), they may damage crop plants unless they are accurately guided.

Robotic weeding becomes possible due to the evolution of perception systems, especially computer vision technology. Research in computer vision for plant sensing has been documented over the past three decades and has led to the development of some robotic weeding machines. For instance, the Garford Robocrop InRow Weeder (Tillett, Hague, Grundy, & Dedousis, 2008) detected crop

plants with a color camera, and guided the disk hoes with a specially designed cutout to cut weeds around the detected crop plants. The Ladybird (Underwood et al., 2015) was a mobile robot that used various sensors such as light detection and ranging (LiDAR), hyperspectral imagers, and GPS for detecting and locating weeds. A six-degree-of-freedom robot arm with a spot sprayer was controlled accordingly. The Deepfield Bonirob (Lottes, Hörferlin, Sander, & Stachniss, 2017; Ruckelshausen et al., 2009) detected crop plants with various of sensors (near-infrared [NIR], RGB cameras, or time-of-flight [TOF] cameras), and treated weeds individually with a stamping tube. The AgBotII (Bawden et al., 2017) detected and classified weeds with a color camera, and control weeds with spot sprayers or hoeing tools.

Among the mechanical robotic weeding solutions, weeding efficacy can still be improved with better actuator design. As a part of this project, a new weeding actuator design for mechanical weeding for row crops and for multiple crop species was developed. The actuator was designed as an implement of a tractor. It employs rotating vertical tines as the weeding tool for effectively cutting, uprooting, and burying weeds (Figure 1). The positioning of the tines was controlled by servomotor-driven pivoting arms. After detecting and localizing crop plants, the tines were controlled to move close to crop row to remove weed plants regardless of their species while avoiding crop plant disturbance and damage.

In robotic weeding, precisely detecting, differentiating and localizing crop plants and weeds is still a challenging task. Feature-based supervised classification is a widely adopted technique in which computers usually use probability functions from digitized features in images to predict categories of objects. Since the shapes of plants are complex and varied, an effective and robust descriptor must differentiate different crop species from different weed plant species in images. More exploration is needed in this field.

Images for plant detection applications are commonly taken by two types of cameras. One type measures the intensity of light reflected from objects onto a discretized image plane. The other type of camera measures the distance between objects in the three-dimensional field-of-view and the sensor, and projects this range information onto an image plane.

Historically, most computer vision-based weed perception systems have used light reflectance images without depth information to identify plants (Slaughter, Giles, & Downey, 2008). Some work has

focused on the different spectral reflectance features of plants and soil to distinguish between them. For example, the excess green index (ExG) and hue saturation value (HSV) color space were found effective in enhancing green plants in standard RGB images (Andújar, Weis, & Gerhards, 2012; Foglia & Reina, 2006; Philipp & Rath, 2002; Tang, Tian, & Steward, 2000). The normalized difference vegetation index, which is a function of the NIR and visible reflectance, was widely used in vegetation pixels segmentation when NIR sensors are available (Gerhards & Christensen, 2003).

After segmentation of images with spectral reflectance data, some approaches extracted engineered features representing the morphology of plant leaves and plant canopies for plant discrimination. These morphological features including length, width, perimeter dimensions, roundness, circularity, convexity, and moment of plant leaves or plant canopy were widely used for feature-based plant identification (Dyrmann, Christiansen, & Midtiby, 2018; Tang & Tian, 2008; Wu et al., 2007). Other than these features, general image features extractors such as scale-invariant feature transform, features from accelerated segment test, histogram of gradient, local binary pattern, and Gabor wavelet transformation, which are descriptors of local textures and key points, were also found effective in plant detection and discrimination, and robust to illumination variations (Bawden et al., 2017; dos Santos Ferreira, Matte Freitas, Gonçalves da Silva, Pistori, & Theophilo Folhes, 2017; Tang, Tian, & Steward, 2003).

In general, it is challenging for traditional methods with light reflectance sensors alone to obtain high discrimination accuracy under highly variable conditions, unless light was controlled and plants were sparse (Slaughter et al., 2008). Since most color cameras are passive receivers of reflected light, they are dependent on the quality of the reflected light received. The color similarity of vegetation pixels can lead to difficulties in separating leaves or plants with occlusions, and uncontrolled illumination can cause shadow effects or saturation effects in images. Features extracted with such conditions may be incorrect and lead to incorrect plant identification results.

More recently, convolutional neural networks (CNNs) in deep learning have been applied in agricultural applications. The main advantage of CNN is the high performance in object detection and automated feature engineering. CNN models such as Inception-v3 (Szegedy, Vanhoucke, Ioffe, Shlens, & Wojna, 2015), GoogleNet

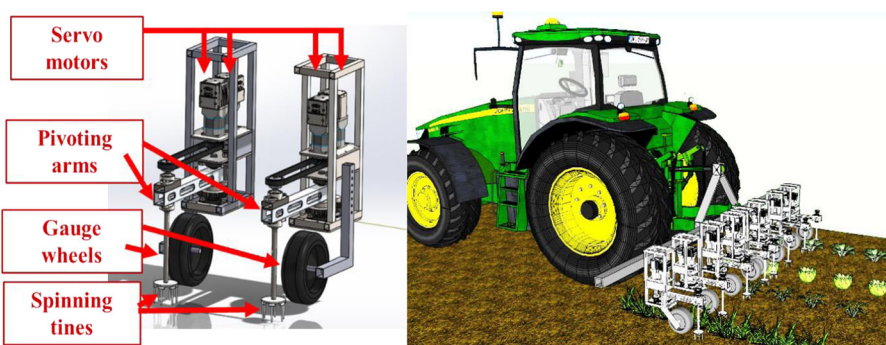


FIGURE 1 The actuators (left) were designed as an implement of a tractor (right), employing rotating vertical tines as the weeding tool for effectively cutting, uprooting, and burying weeds [Color figure can be viewed at wileyonlinelibrary.com]

(Szegedy et al., 2014), DenseNet (Huang, Liu, Van Der Maaten, & Weinberger, 2017), and customized models were proven effective in crop/weed detection and classification even with uncontrolled illumination (Dyrmann, Jørgensen, & Midtiby, 2017; Dyrmann, Karstoft, & Midtiby, 2016; McCool, Perez, & Upcroft, 2017; Milioto, Lottes, & Stachniss, 2017; Potena, Nardi, & Pretto, 2017).

CNN approaches, however, also face several challenges. First, deep learning requires high computational capacity for training and real-time inferencing. Second, deep learning has not been well integrated with prior knowledge so far, and it is difficult to engineer with, as indicated by Marcus (2018). The performance of deep learning depends on the quality of the datasets more than other conventional machine learning methods. The training data set size must be sufficiently large to prevent overfitting, and that requires substantial manual labor to collect and annotate images. Also, the data set must span all conditions such as inconsistent illumination, shadow and occlusion to improve robustness (Kamilaris & Prenafeta-Boldú, 2018). Thus, investigations of traditional pattern recognition pipelines are valuable and can provide a complementary approach particularly for applications with limited computational capacity and available datasets.

Range information, which reflects the 3D shape of objects, were found promising in addressing some of the problems in plant identification associated with color-based sensors alone. Specifically, 3D plant features such as edges and curvatures extracted from the 3D point cloud are more robust to external illumination condition changes than those extracted from color images. In addition, plant height can be an effective discriminating parameter between crop and weeds at early crop growth stages (Piron, van der Heijden, & Destain, 2011), which can be used for crop/weed segmentation and classification. Studies of crop or weed plant detection using range data have been reported. Three types of state-of-the-art range sensors were commonly used in agricultural applications, including stereo-vision, LiDAR, and TOF sensors (Weiss, Biber, Laible, Bohlmann, & Zell, 2010). Stereo-vision extracts the distance between the sensor and objects in the field-of-view using images acquired with multiple cameras and exploits advantages of high image resolution, available color information, and detailed textural information (Kise, Zhang, & Rovira Más, 2005), while challenged by sensitivity to illumination and high computational requirements (Tippetts, Lee, Lillywhite, & Archibald, 2016). Jin and Tang (2009) demonstrated the use of a real-time stereo-vision system for corn seedling detection, in which the structural features of corn plants were extracted to identify the stem location of the corn plants at V2-V3 growth stages. Cameras with range sensors such as TOF sensors and LiDAR sensors measure distance based on the time difference between transmission and reception of typical infrared light signals. The active sensing mode makes these range cameras more robust to varying outdoor lighting conditions. In the work of Weiss and Biber (2011), a robot (Deepfield Bonirob) was equipped with a LiDAR sensor to effectively map outdoor maize plants. Li and Tang (2018) developed a TOF camera-based perception system for crop plant detection. Features such as curvature, normal, and neighbor counts were extracted from the 3D point cloud to detect broccoli and green bean leaves.

Since both color and range data can be beneficial, the fusion of color and depth images was explored for in-field crop/weed discrimination. Each image type has complementary information. Common sensors are color and depth sensors with calibrated extrinsic parameters (Herrera, Kannala, & Heikkila, 2012), or commercial RGB-D camera such as Kinect (Microsoft, Redmond, WA), which directly outputs registered RGB color and depth information. The benefits of fusing color and range data were demonstrated in some agricultural applications. Nguyen et al. (2016) employed an RGB-D sensor to detect apples, in which 3D information was used for segmentation and clustering and color information was used to detect apples after circular Hough Transformation. In the study of Sa et al. (2017), an RGB-D sensor was used to detect sweet pepper peduncles for robotic harvesting. Kusumam, Krajník, Pearson, Duckett, and Cielniak (2017) developed a mature broccoli head detection algorithm using an RGB-D sensor for robotic harvesting, and obtained a high detection rate. Xia, Hwang, Lee, Lee, and Lee (2015) developed an algorithm to segment pepper leaves from complex background in greenhouses using a Kinect sensor. Andújar et al. (2016) employed a Kinect v2 sensor to estimate weed densities in corn fields. However, no studies reported on the fusion of color and depth to detect crop plants of multiple growth stages for the purpose of robotic weed control.

In this study, the benefits of fusing color and depth in crop plant segmentation for the automated weeding application was demonstrated. And a novel image processing pipeline for crop plant detection and localization by fusing color and depth images was developed and evaluated. The pipeline is adaptable to weeding robots which need to detect crop plants, such as in our design (Figure 1) and the Robocrop Weeder (Tillett et al., 2008). The image processing pipeline consists of several steps including data pre-processing, vegetation pixel segmentation, plant extraction, feature extraction, feature-based localization refinement, and crop plant classification. The algorithm is robust to high-density weeds. The primary objective of this paper was to evaluate the performance of the proposed pipeline in detecting and localizing crop plants at different growth stages. Specific research objectives were to:

- verify the fusion-based strategy will improve the segmentation performance compared with using color or depth only,
- evaluate the performance of the proposed fusion-based crop plant detection and localization algorithm at different critical processing steps, including segmentation, individual plant detection, and feature-based classification.

2 | SENSOR AND DATA COLLECTION

2.1 | Sensor

An RGB-D sensor (Kinect version 2; Microsoft) was used in this study, which provides color (RGB), infrared reflectance intensity and depth information. Depth was sensed using a semiconductor-based PMD

(Photonic Mixer Device) TOF chip. The sensor contains three strong infrared light emitters, which enables the sensor to function under outdoor conditions when sunlight is not strong or has been reduced in intensity by shading. The sensing system outputs high-resolution RGB images at a $1,920 \times 1,080$ pixel spatial resolution, as well as infrared intensity and depth images at a 512×424 pixel resolution at 30 frames per second. At an outdoor working distance of 0.75–1.25 m with shaded sunlight, the standard deviation of the depth measurements was within 4 mm (Fankhauser et al., 2015). The systematic errors of Kinect v2 depth measurements including depth distortion, amplitude-related error, temperature-related error, and material-related error were estimated to be ± 1 mm theoretically in this study (Corti, Giancola, Mainetti, & Sala, 2016; Fankhauser et al., 2015). Overall, the depth measurement uncertainty of the Kinect v2 sensor is within 5 mm (68% confidence level) by summing up the nonsystematic errors and systematic errors.

2.2 | Data collection

The target crop species analyzed were two common vegetable crops: lettuce (*Lactuca*, L.) and broccoli (*Brassica oleracea* L. var. *botrytis* L.). Various types of weeds that are common in Iowa were also in the scene, including bromegrass (*Bromus inermis* Leyss), pigweed (*Amaranthus* spp.), lambsquarters (*Chenopodium album*), waterhemp (*Amaranthus rudis*), barnyardgrass (*Echinochloa crus-galli*), bindweed (*Convolvulus arvensis*), purslane (*Portulaca oleracea*), and white clover (*Trifolium repens*).

A data collection system, consisting of a Kinect v2 sensor and a laptop computer, was built on a remote-controlled ground vehicle (Figure 2). The sensor was placed about 0.75 m above the plants. With the selected working distance, the spatial resolution of depth was about 2 mm/pixel (12.5 ppi) in both vertical and horizontal directions while measuring the plants. The field of view was about 0.89 m (~34") in vertical direction and 1.05 m (~41") in horizontal direction (Figure 3).



FIGURE 2 Remote-controlled data collection apparatus in the horticulture research station of Iowa State University [Color figure can be viewed at wileyonlinelibrary.com]

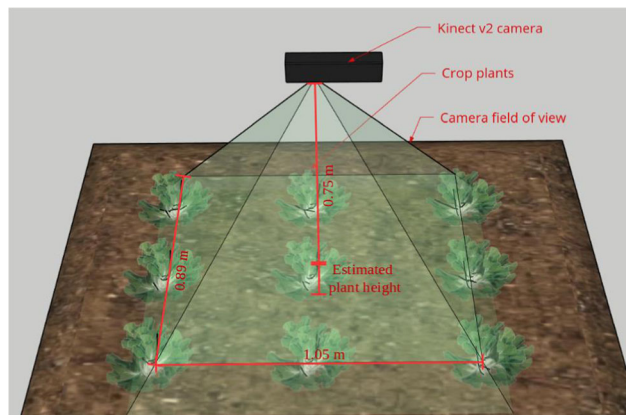


FIGURE 3 The Kinect sensor was mounted at 0.75 m plus the estimated plant height above the field surface and had a 1.05 m \times 0.89 m field of view of the plants and soil below [Color figure can be viewed at wileyonlinelibrary.com]

Data were acquired at the Horticulture Research Station of Iowa State University in Story County (42.11°N , -93.59°E). The soil was close to Shunk River and nearly level. Soil type was mostly Clarion loam, moderately eroded, with a 5% to 9% slope. The average annual temperature was 49.45°F and the average annual precipitation was 0.91 m (35.83"). The crop plants used in this study (about 40 plants for each species) were started in a greenhouse and transplanted at the Horticulture Research Station. The row spacing was 0.76 m (30"), and the interrow plant spacing was 0.3 m (12"). Weeding on the field was not fully performed to collect crop plant images from weed infested crop fields. The weed coverage was ranged from 5% to 50% of the imaged area.

Data were acquired with a Kinect v2 sensor in the summers of 2015 and 2016. For each crop plant species, images were taken at daytime about every 5 days from the date of transplanting to maturity. More than 3,000 images were taken for each species. An umbrella was used to block the sunlight in sunny days to reduce the illuminance from above 80,000 lux to about 9,000 lux. In cloudy days, the average illuminance was about 35,000 lux, and no umbrella was used. Top view images were acquired every 0.3 m along the crop rows with the customized data collection system, and an overlap of 0.6 m between adjacent images was obtained. Depth images, near-infrared reflectance intensity images, and color images were acquired.

3 | ALGORITHM DESIGN

The acquired depth images from the depth sensor and RGB color images from the color camera were used as the inputs to the image processing algorithm. The framework of the detection and localization algorithm is shown in the flowchart (Figure 4) and can be outlined in the following steps:

Step 1. Preprocessing: This procedure removed invalid pixels and noise pixels in point clouds. A useable-area filter, a cutoff filter, and a simplified neighbor count filter were used.

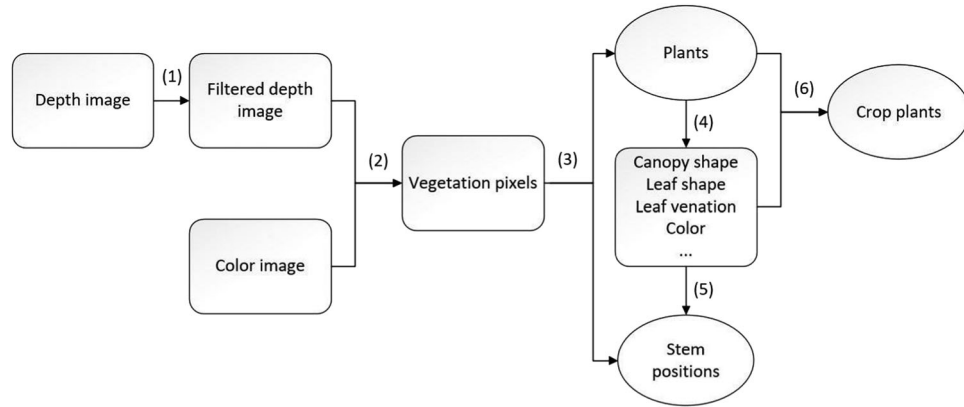


FIGURE 4 Data flow diagram of the image processing algorithm. Each of the numbers corresponds to one of the image processing steps listed above

Step 2. Segmentation: The background was removed by detecting the soil surface (assumed to be a plane) using both color and depth information. Vegetation pixels were extracted.

Step 3. Plant extraction: The vegetation pixels were separated into different clusters using their spatial relationship. Each cluster represented one individual plant. These plants were localized as well.

Step 4. Feature extraction: Canopy and leaf features of each detected plant were extracted.

Step 5. Feature-based localization refinement: The extracted features were used for refining the localization and extraction results.

Step 6. Classification: Crop/weed classification was applied to all the separated plants based on their extracted features using machine learning techniques.

The algorithm was tuned and tested with broccoli and lettuce datasets collected at different growth stages with weeds of different species and at different infestation levels. Each of these steps will be further described in the following sections.

3.1 | Preprocessing on depth images

The raw depth images collected outdoor by the Kinect v2 sensor contained a substantial amount of noise (Figure 5). In this algorithm, three simple filters were applied sequentially on the depth image to reduce the image noise level.

3.1.1 | Useable-area filter

Because of the ambient light effect on sensor performance, off-center pixels in depth images were more likely to carry incorrect depth information (Figure 5). In this study, the pixels within a round area centered at the image center with a 220 pixel radius were found

reliable. The rest of the area in the depth images were discarded. This filtering operation was expressed as

$$dst(x, y) = \begin{cases} src(x, y) & \text{if } \|(x, y) - (256, 212)\| < 220, \\ 0 & \text{otherwise,} \end{cases} \quad (1)$$

where $src(x, y)$ is a pixel value in source depth image at position (column, row), and $dst(x, y)$ is for a pixel in destination depth image. Position (256, 212) is the estimated principal point position of the camera. In this process, about 30% of the points were discarded.

3.1.2 | Depth cutoff filter

Invalid pixels (zero or infinity value) and pixels with large depth values (noise in most cases) were removed by using this filter. Through testing, a high threshold of the sensor height plus 200 mm was found robust to ensure the ground can be reserved. The low threshold was selected to be 500 mm, which is also the minimum working distance of the Kinect v2. The operation was expressed as



FIGURE 5 A sample depth image of broccoli indicating the depth (z-direction distance). The noise level was higher in the off-center area, especially at corners. Units are in mm from the sensor

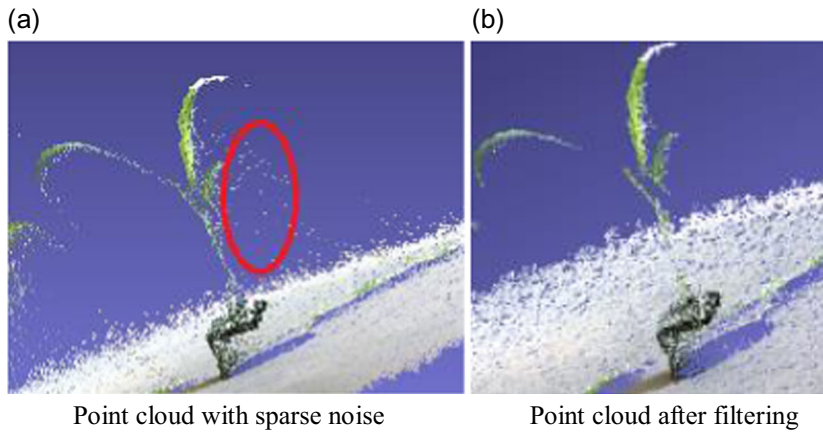


FIGURE 6 Corn plant sample images showing the differences before (a) and after (b) preprocessing. The point clouds were generated from corn plants in the laboratory to illustrate the filtering process. After applying preprocessing procedure, the sparse noise was removed [Color figure can be viewed at [wileyonlinelibrary.com](#)]

$$dst(x, y) = \begin{cases} src(x, y) & \text{if } 500 < src(x, y) < h + 200, \\ 0 & \text{otherwise,} \end{cases} \quad (2)$$

where (x, y) is the position of a pixel, and h is the sensor height in millimeter above the ground when taking this image.

3.1.3 | Neighbor count filter

The Kinect v2 depth sensor generates “flying pixels” at the edges of imaged objects (Figure 6), which are similar to blurred edges in 2D images. These pixels are sparse and have fewer “neighbors” in 3D space.

Since the output of the depth sensor of Kinect v2 was organized in rows and columns, simplified local radius-based neighbor search was used to count neighbors in this study, which limited the searching process within a window in the images space of the depth image. The complexity was $O(1)$, which is lower than the average complexity of $O(\log n)$ global k-d tree-based 3D searching algorithms. A window size of 5×5 was selected, and pixels that had horizontal distance (along the depth measurement direction) less than 15 mm were considered as adjacent pixels.

During filtering, neighbors for each pixel were calculated, then pixels with less than 15 neighbors were removed. This threshold was

selected for a 5×5 searching window ensuring pixels on the edge were retained. The filtering operation were expressed as

$$dst(x, y) = \begin{cases} src(x, y) & \text{if } RNS(x, y) > 15, \\ 0 & \text{otherwise.} \end{cases} \quad (3)$$

3.2 | Segmentation using depth and color

In segmentation, pixels were divided into two different subsets: vegetation pixels, and background pixels. With the depth information available, the main strategy of segmentation was to find the ground plane in the point cloud using random sample consensus (RANSAC) (Weiss & Biber, 2011). RANSAC is widely used for model fitting with outliers (Figure 7a). It iteratively samples three random points in the point cloud to form a plane, and select the best plane with the least outliers. The model was refined with linear least squares regression. In fitting the ground plane, the soil surface should be inliers and the vegetation pixels should be outliers (Figure 7b). However, when too many outlier points from plants are present, the original RANSAC will find an incorrect ground plane. To address this problem, a color-weighted RANSAC algorithm was developed in this study based on the original RANSAC to increase the accuracy of ground fitting.

In the segmentation algorithm, instead of using outlier count to evaluate the modeled ground surface planes from the original RANSAC,

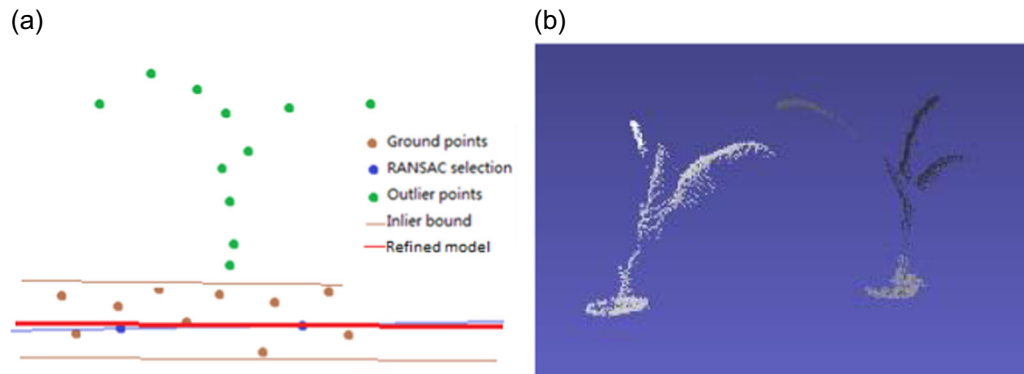


FIGURE 7 (a) A synthetic 2D point cloud of a plant with a RANSAC-fitted plane to visualize the principle of the ground detection. Two points were randomly selected (blue), and a line was fit to these points (blue line). Then the fitted plane was refined using linear regression (red line). The points between the brown lines were inliers from the ground. (b) A sample point cloud with only outliers after ground detection. The points of the ground were successfully removed [Color figure can be viewed at [wileyonlinelibrary.com](#)]

the color-weighted distance \hat{d}_i was summed among all points in the point cloud to calculate the cost of each fitted plane:

$$\text{cost} = \sum \hat{d}_i = \sum \text{weight}(\mathbf{p}_i) \times d(\mathbf{p}_i, \mathbf{n}), \quad (4)$$

in which the registered color value of point \mathbf{p}_i formed a weight factor, indicating the importance of each pixel in fitting the ground, and $d(\mathbf{p}_i, \mathbf{n})$ is the distance in 3D space from point \mathbf{p}_i to plane \mathbf{n} . Higher weights were expected for the ground pixels while fitting the ground, which should be the inliers in ground fitting. Lower weights were expected for the vegetation pixels, which should be the outliers that are less impactful in ground fitting. After fitting the ground plane, the outlier pixels were extracted by using the distance of the points divided by their calculated weight factors, to distinguish the vegetation pixels and background in height.

The weight function of Equation (4) was defined as

$$\text{weight}(\mathbf{p}_i) = 1 + P(\mathbf{p}_i \in \text{Ground}), \quad (5)$$

in which $P(\mathbf{p}_i \in \text{Ground})$ indicates the probability of "pixel \mathbf{p}_i belongs to the ground pixel set," as a function of the color of the point.

A reliable color index was needed to represent the difference between background and vegetation pixels while being resilient to illumination changes. The illuminant-invariant (ill-inv) maps created based on the illuminant-invariant color space (Finlayson, Hordley, & Drew, 2002) were found able to reduce the shadow effects within the original color image (Figure 8). The HSV color space was also found reliable to distinguish green plants from the background (Hamuda, Mc Ginley, Glavin, & Jones, 2017). Thus, both ill-inv maps and the HSV color space image were selected to be candidates for calculating the weights.

In this study, a logistic regression model with a sigmoid shape was used to determine the probability density function (PDF), which is expressed as

$$P[Y = 1 | X = \mathbf{x}_i] = \frac{e^{(\beta_0 + \beta_1 \mathbf{x}_i)}}{1 + e^{(\beta_0 + \beta_1 \mathbf{x}_i)}} = \frac{1}{1 + \exp(-\beta_0 - \beta_1 \mathbf{x}_i)}, \quad (6)$$

and could transform the color information into a 0–1 range. Scalar β_0 and vector β_1 are the coefficients, and \mathbf{x}_i is a vector variable representing the

color. The logistic regression was used for two reasons. First, the logistic response function curve is monotonically increasing or decreasing depending on the signs of β_1 . The curve gradually approaches 0 and 1 after being approximately linear in the middle. Secondly, the logistic response function model is based on maximum likelihood estimation theory, and does not rely on the assumptions of normally distributed error, equal variance of different parameters of data, and independently and identically distributed data which may not characterize the data. In addition, this model has a relatively low computational cost in fitting the model and calculating the probability.

For simplicity, the color vector variable \mathbf{x}_i in Equation (6) was selected from one of three color spaces: RGB, HSV, and illuminant-invariant. By analyzing the images acquired with our data collection system statistically (Gai, 2016), the most effective color space in distinguishing plants and soil surface were selected. The models of Equation (6) were fitted individually for broccoli and lettuce using the corresponding image set during the training phase, and used for segmentation during testing. With the data set collected in this study, the RGB and the illuminant-invariant color spaces were the most effective ones in plant segmentation for broccoli and lettuce, respectively. However, this may subject to change with the system working conditions such as soil types and shading methods.

3.3 | Plant extraction

Segmented vegetation pixels were grouped into clusters representing individual plants based on the spatial relationship of pixels. In this step, an above-ground distance map was created, which replaced the values of the input depth image with the distance of each corresponding point to the modeled ground plane. Clustering was applied on the created above-ground distance map, and the problem was reduced to a 2D unsupervised clustering problem on an image.

A 2D connected components method, which used a region growing schema, was used on the output mask of the segmentation step first for coarse clustering. After that, an algorithm based on the two-dimensional multiscale wavelet transformation was applied on the above-ground distance map with a mask of the segmentation result, using prior knowledge of the shape patterns of crop plants. The Mexican hat wavelet

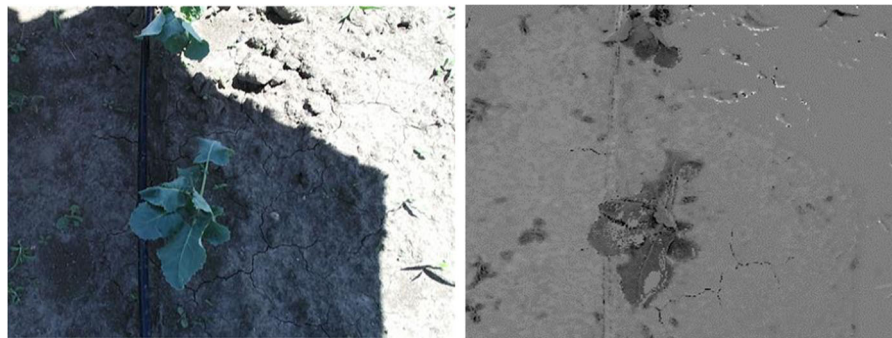


FIGURE 8 Sample illuminant-invariant map. In the left figure, the lighting conditions were different between the shaded and unshaded areas. In the right figure, the illuminant-invariant map was generated and removed the effects of changing lighting conditions. Green pixels had lower values in illuminant-invariant maps [Color figure can be viewed at wileyonlinelibrary.com]

was found effective in extracting shape patterns that are in spherical shape and isotropic. The normalized Mexican hat wavelet was defined as

$$z = (2 - (x^2 + y^2)/s^2) \times \exp\left(-\frac{x^2 + y^2}{2s^2}\right)/ s^2, \quad (7)$$

in which parameter s is a scale factor, indicating the wavelet size. The fast Fourier transform was used to reduce the computational cost of convolutions.

The wavelet transformation results at different scales were analyzed. The local extremes corresponded to the stem locations of individual crop plants, and the scales with maximum response at these local extremes corresponded to the plant canopy sizes. Vegetation pixels were associated with different clusters based on the plant stem locations and canopy sizes. These clusters indicated individual plants but without being labeled by their species tags yet.

Additionally, for plants without a spherical shape or not isotropic (eg, the broccoli 13 days after transplanting [DAT] in this study), the plant extraction and localization will be refined using features extracted in the later steps.

3.4 | Feature extraction

Plant discrimination was accomplished by feature-based classification. In this study, a series of hand-crafted features which represent the morphology and structure of plant canopies and leaves were extracted. In this section, the leaf and canopy features with their extraction methods are listed. Explicitly, the leaf extraction method and the leaf venation feature extraction method are stated in detail.

3.4.1 | Plant features

Inspired by the research of Wu et al. (2007), a set of morphological and structural features of plant leaves and canopies was selected in this study based on the consideration of feature distinguishability and algorithm simplicity. A program was developed to automatically extract the following features:

1. Leaf venation, which is a Boolean variable, indicating whether the venation of the leaf can be extracted. The extraction method will be stated in the following section.
2. Leaf height, which is the distance between the fitted ground and the centroid of the leaf.
3. Leaf area, which is the area of the leaf after projected to the ground plane.
4. Leaf length, which is the maximum length on the leaf measured in 3D.
5. Leaf width, which is the width of the leaf, perpendicular to the length direction, measured in 3D.
6. Leaf aspect ratio, which is the ratio between the length of the leaf, and width of the leaf.

7. Leaf roundness, which is the ratio between the leaf contour length and the bounding ellipse circumference, measured inside the image plane.
8. Leaf rectangularity, which is the ratio between the leaf area and the leaf's bounding rectangle area, measured inside the image plane.
9. Leaf hue, which is the average hue value in the HSV color space of the leaf pixels.
10. Leaf saturation, which is the average saturation value in the HSV color space of the leaf pixels.
11. Leaf illuminant-invariant value, which is the average ill-inv value of the leaf pixels.
12. Canopy height, which is the maximum distance from the ground plane to the highest point of the plant.
13. Canopy radius, which is the size of the bounding circle of the canopy measured in 3D.
14. Leaf number, which is the number of leaves that can be segmented from the plant data.
15. Canopy hue, which is the average value of the hue channel in the HSV color space of the canopy pixels.
16. Canopy saturation, which is the average value of the saturation channel in the HSV color space of the canopy pixels.
17. Canopy illuminant-invariant value, which is the average illuminant-invariant value of the plant points.

3.4.2 | Leaf segmentation

Each leaf in the extracted plants was segmented to extract the leaf features (features 1–11). The marker-controlled watershed segmentation algorithm (Shafarenko, Petrou, & Kittler, 1997) was applied to both depth images and color images, specifically the HSV hue channel, to segment leaves. This general segmentation algorithm was used instead of using leaf shape as prior knowledge, because leaf damage was common in the data set collected, and the leaf shape patterns were not always available.

The “watersheds” in this study were the edges of leaves. The edges were defined by the discontinuities in depth and color. Those discontinuities were detected using the magnitudes of gradients in these images. In image processing, those partial derivatives were approximated by convolving Sobel operators to images for horizontal and vertical derivatives, respectively. The magnitude of the gradient became the root of the square sums of the derivatives.

The label seed map was obtained from distance transformation to the edge map. The area with distance to the closest edges greater than a threshold was labeled with one of the foreground labels (label n , $n > 2$). The pixels identified as background in previous steps were labeled as background (Label 0). The rest of the pixels were labeled as unknown (Label 1).

Then, the flooding algorithm was applied to the depth and color images, as well as the label seed map. An example resultant label image is shown in Figure 9. Based on the segmentation results, features 2–11 can be extracted by analyzing the shape and color of each segment.

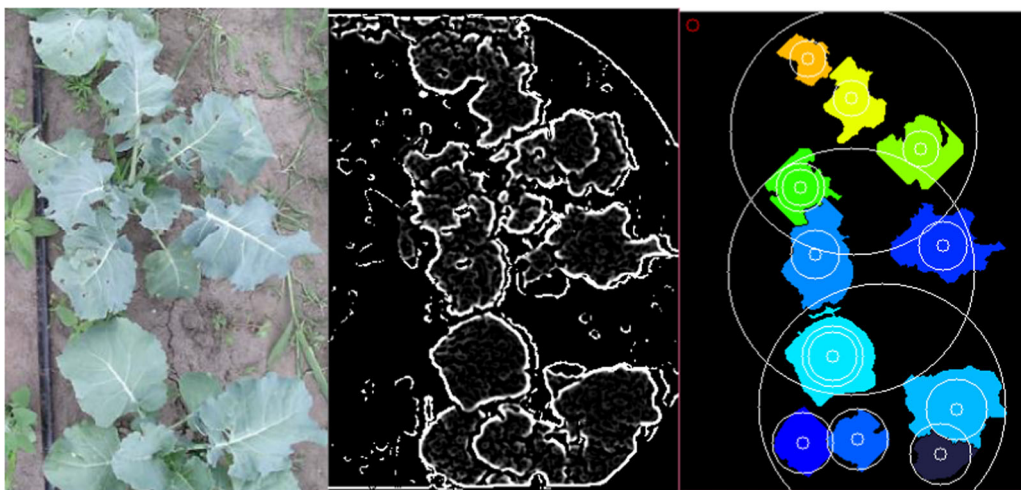


FIGURE 9 A runtime output example showing the leaf extraction procedures. Left, color image from broccoli, with connected plants, slightly occlusions, as well as broken leaves. Middle, combined gradient magnitude image on both color and depth. Right, leaves extraction result example. Most of the leaves were extracted and labeled with different colors [Color figure can be viewed at wileyonlinelibrary.com]

3.4.3 | Venation extraction

Venation (feature 1), as a leaf feature, was a distinguishing feature for crop plant detection. It was resilient to most leaf damage and is a robust feature to determine the direction of leaves. As the pixels from veins usually have higher intensity in color images compared to surrounding pixels, those vein pixels were considered as “ridges” in the images. Ridge detection technique was applied to the color images. By limiting the processing areas to those leaves’ areas (obtained in leaf segmentation step), the veins were extracted, and a thinning algorithm (Chen & Hsu, 1988) was applied to skeletonize the veins (Figure 10).

3.5 | Feature-based localization refinement

In this step, the localization of plants in images was refined based on the features extracted, especially the venations. A novel algorithm was developed in this study. Based on the observation that leaves of broccoli and lettuce plants are growing in pattern that radiates from the center of the canopy in top views, and thus the stems or the centers of the plants were localized by analyzing the leaves’ directions. Plant extraction results were refined by assigning extracted leaves to plants based on the leaves’ directions and their distances to the plant center.

Primary veins were found to be a reliable indicator of the leaves’ direction, and the stem location lies on the extension lines of the

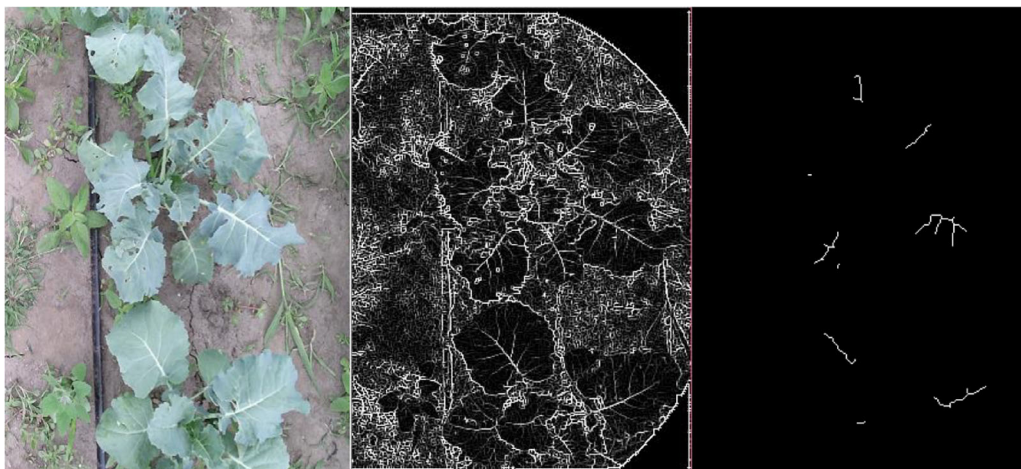


FIGURE 10 An example runtime output of venation extraction methods. The left image is the raw image collected from the broccoli field. Leaf venation was found to be a robust feature to detect broccoli plants. The middle figure shows the map of reversed lower eigenvalues of Hessian matrices of each pixel. Ridge pixels have higher intensity in the map. The right figure shows the extracted and skeletonized veins [Color figure can be viewed at wileyonlinelibrary.com]

primary veins. Based on these observations, an algorithm was developed to find the plant stem location using venations. The stem localization algorithm consisted of three steps:

1. Find all the vein branches, and fit line segments to them using least squares regression.
2. Estimate the probability of a line segment being a primary vein of a leaf, and assign a weight factor to each line segment based on the probability.
3. Solve the center-finding problem by using the weighted robust least square method.

In the first step, all the branches were separated by finding joints and fitting line segments using least squares regression. In many binary skeletonizing algorithms with small thinning windows, the joints always follow some common patterns. For instance, in the algorithm of Chen and Hsu (1988) all the joints were formed by patterns of either "Y"s or "T"s. After the joints were found, the vein branches/segments were separated.

The second step was to assign each line segment a weight factor, to reflect the probability of being a primary vein of a leaf. In most cases, a primary vein is the longest and has the most joints on it. In this step, for each line segment, the online joint count c was determined by counting joints who lie in the same leaf and have vertical distances less than five pixels to the line segment. Then the weight factor of each line segment was defined as the product of line segment length and a normalization function of online joint count c . The weight factor was defined as

$$\text{weight} = \text{line segment length} \times \frac{\max(1, 3 \times c)}{\max(1, 3 \times c_{\max})}, \quad (8)$$

where c_{\max} is the maximum online joint count found within the current leaf.

In the last step, an iterative weighted least square algorithm was used to find the stem location by finding a point who has minimum vertical distances to all the fitted line segments from primary veins. It iteratively activated and deactivated each line segment to ensure only inliers (ideally the primary veins) were used for fitting. For each iteration, the inlier line segments were activated, and the outlier line segments were deactivated. Then the center point was calculated by a weighted least square method, which solves

$$\mathbf{p} = \underset{\mathbf{p}}{\operatorname{argmin}} \sum_j (w \times \text{dis}(\mathbf{p}, I_j))^2, \quad (9)$$

where \mathbf{p} is the center point, I_j is the j th activated line segment. With the new calculated center, the distance of each line segment to the new center point was calculated. The mean and the standard deviation of the distances were calculated. Based on the mean and the standard deviation the line segments with longer distance to the center point were labeled as outliers, and deactivated in the next iteration. The iterations continued until the center point reached the desired accuracy. An example runtime output was shown in Figure 11.

3.6 | Feature-based classification

Features extracted in the previous steps were used for crop/noncrop classification of each extracted plant. The classification was in a two-layer scheme, which is similar to the work of Dyrmann et al. (2018). The first layer consisted of a leaf/nonleaf classifier that used leaf features to exclude the incorrectly detected leaves from further classification. After classifying each leaf, for each separated plant, the classified crop leaf parameters were used to form a new set of predictors for the second classification layer. In this study, the statistical values including the maximum, minimum, mean, median, and standard deviation of each leaf feature in the same plant were formed as new predictor variables. The second layer was a crop/noncrop classifier that used the canopy features and the leaf features from classified leaves to classify each detected plant into the crop plant class or the noncrop plant class.

Among leaf features and canopy features, some features were found correlated. Principal component analysis was performed to reduce the dimension of these features before fitting models.

Eight supervised machine learning classification algorithms were applied to the features extracted in the training phase. These algorithms were logistic regression (LR), k -nearest neighbors (KNN), artificial neural network (ANN), Bayes classifiers such as linear and quadrature discriminant analysis (LDA and QDA), the support vector machine (SVM), and tree-based classifiers such as random forest (RF) and adaptive boosting (Adaboost). Then those models were evaluated by using cross-validation (CV) results. The image processing algorithm was implemented being written in C++ with calls to

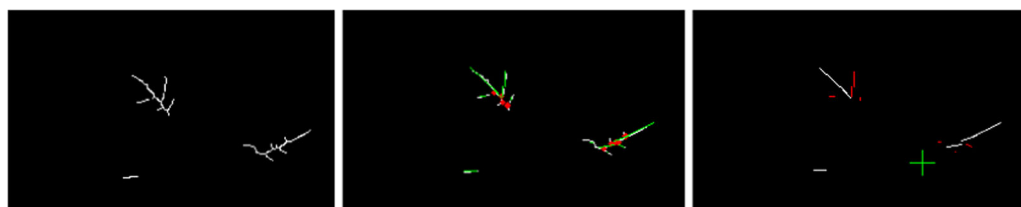


FIGURE 11 A runtime output example of stem localization. (Left) The venation skeletons of the lowest plant in Figure 10. (Middle) The joints are colored in red, and the fitted line segments are drawn in green, with their lengths proportional to their weight factors. (Right) The green cross indicates the resultant center location in the current iteration. The line segments with white color are the active (inliers, with nonzero weights in current iteration) [Color figure can be viewed at wileyonlinelibrary.com]

methods in the OpenCV library. The classification evaluation program was implemented using R language.

4 | EXPERIMENTAL DESIGN

The image analysis algorithm was applied, and the parameters were tuned with our broccoli and lettuce datasets collected in year 2015 and 2016. The performance of the developed algorithm was evaluated in terms of the accuracy of accomplishing three critical steps: segmentation, plant detection and localization, and classification. The evaluation image set contained randomly selected 100 images for each species at five image collection time periods (3–7, 8–12, 13–17, 18–22, and 23–27 DAT), for a total of 500 images for each species. The crop plant pixels and the crop plant stem locations in the evaluation image set were manually labeled for algorithm testing. The segmentation, plant detection, and localization algorithms (Steps 1 through 5 in Figure 4) were evaluated using the labeled evaluation image set. For classification (Step 6 in Figure 4), the models were trained using features from all the plants extracted after applying plant extraction algorithm (Steps 1–5) to the entire image set, and evaluated using CV.

4.1 | Segmentation performance

Segmentation performance (after Step 2) was characterized by “segmentation success rate,” which is defined as the percentage of evaluation images segmented with intersection over union (IoU) greater than 75% (Long, Shelhamer, & Darrell, 2015). IoU greater than 75% indicates the ground plane was found correctly, and pixels from the crop plants were mostly extracted. The IoU was defined as

$$\text{IoU} = \frac{\text{Segmented crop plant pixels} \cap \text{Labeled crop plant pixels}}{\text{Segmented crop plant pixels} \cup \text{Labeled crop plant pixels}}. \quad (10)$$

After applying the segmentation algorithm to preprocessed images, successfully segmented ($\text{IoU} > 75\%$) images of different growth stages were counted and compared.

4.2 | Performance improvement verification

To verify the benefits of fusing depth and color in segmentation, two comparison experiments were conducted. To keep algorithm complexity consistent in the color-based method, the color PDF (Equation (6), with 0.5 as probability threshold) was applied to the color image to classify foreground and background pixels. One PDF function was fit using training data set for each species, individually. The reason of not fitting multiple models for different growth stages was the motivation to test the robustness of the method against inconsistent illumination and other uncontrolled environment parameters. In the depth-based method, the original RANSAC algorithm was applied to the filtered depth image for segmentation. The algorithms were applied to the same data set used by the proposed data fusion algorithm. Their performance was also evaluated using IoU-75%, and compared with the proposed fusion-based algorithm.

4.3 | Plant detection and localization performance

The detection performance (after Step 5) was evaluated by the percentage of the crop plants extracted in the evaluation image set, which is the recall, defined as true positive/(true positive + false negative). Since all the crop plants were expected to be extracted, the Recall was expected to be 100%. The crop plants were characterized as correctly extracted if the IoU was greater than 50%, with which most of the features were found preserved. The localization performance was evaluated by the mean absolute error (MAE), which was calculated by measuring the distance from the localization result to the labeled plant stem location in the image space, then calculated the real-world distances with the 3D point cloud. The error was named as “average crop plant localization error” in the following sections. In this study, the feature-based refinement was applied to

TABLE 1 The segmentation success rate (% of images with $\text{IoU} > 75\%$) of different algorithms for broccoli and lettuce at different growth stages

Days after transplanting		3–7	8–12	13–17	18–22	23–27	Average
Estimated weed coverage (%)		5–10	5–15	15–30	25–45	35–50	
Broccoli	Weather	Cloudy	Cloudy	Cloudy	Cloudy	Sunny	
	Average crop plant height (mm)	120	150	170	220	280	
	Fusion-based algorithm (%)	88	100	100	99	96	96.6
	Depth-based algorithm (%)	68	100	100	81	87	87.2
	Color-based algorithm (%)	100	100	81	84	26	76.4
Lettuce	Weather	Cloudy	Cloudy	Cloudy	Sunny	Sunny	
	Average crop plant height (mm)	90	110	110	120	130	
	Fusion-based algorithm (%)	84	90	100	98	90	92.4
	Depth-based algorithm (%)	54	63	80	91	83	74.2
	Color-based algorithm (%)	100	100	95	52	59	81.2

Note: The human-measured average crop plant heights and weed densities at the corresponding data collection time were listed. The top success rates among the three algorithms for each growth stage and species were highlighted in bold.

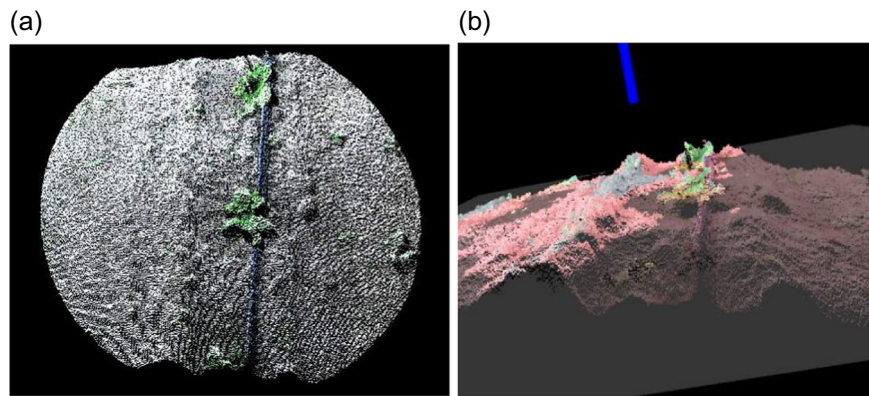


FIGURE 12 A sample failure case of the depth-based algorithm (lettuce, 7 DAT). The algorithm failed to fit the correct ground plane and extract vegetation pixels in the point cloud (a), because the height contrast between soil and plants is not significant. Image (b) displays the segmentation result of the depth-based method. The fitted ground is displayed as a semitransparent plane, and the segmented ground pixels were colored red. The results also cannot be improved by using the proposed fusion-based method [Color figure can be viewed at wileyonlinelibrary.com]

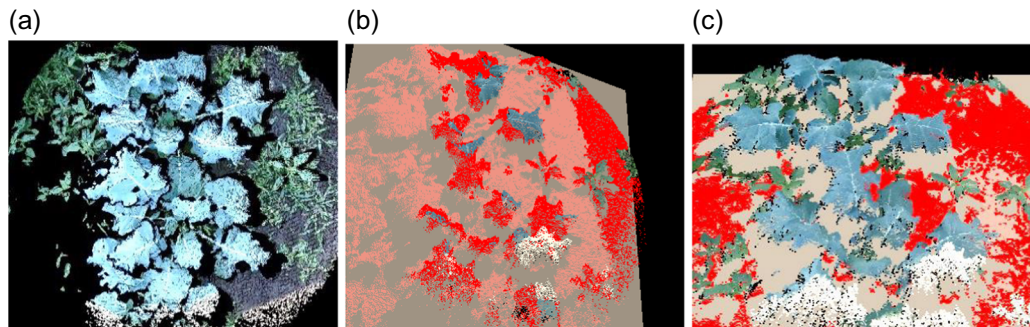


FIGURE 13 A sample failure case of the depth-based algorithm (broccoli, 22 DAT). The algorithm failed to fit the correct ground plane and extract vegetation pixels in the point cloud (a) because of the high weed coverage. Image (b) displays the segmentation result of the depth-based method. Image (c) shows the corresponding improved result from the proposed fusion-based algorithm. The fitted ground is displayed as the yellow (transparent) plane, and the segmented ground pixels were colored red [Color figure can be viewed at wileyonlinelibrary.com]

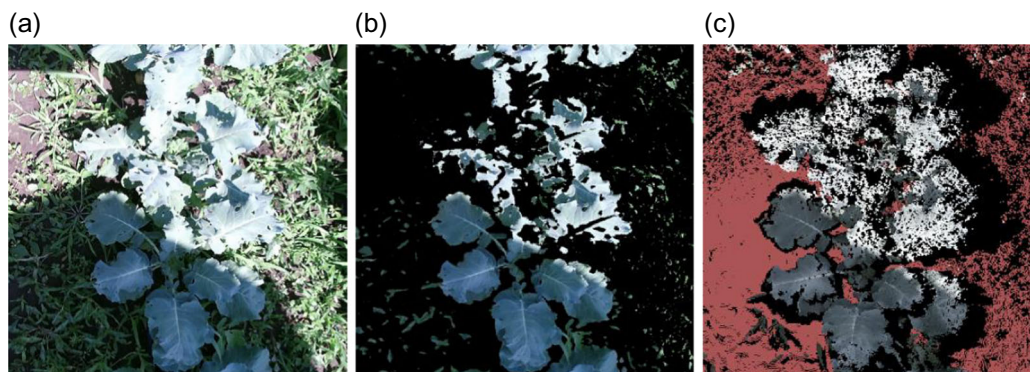


FIGURE 14 A failure case of the color-based algorithm (broccoli, 27 DAT) due to the extreme light conditions and shadow effects in image (a). Image (b) shows the color-based segmentation results, in which many saturated pixels were classified as background. Image (c) shows the corresponding improved result from the proposed fusion-based algorithm as a colored 3D point cloud, in which the color of segmented background pixels were colored red, and the color of vegetation pixels remain unchanged [Color figure can be viewed at wileyonlinelibrary.com]

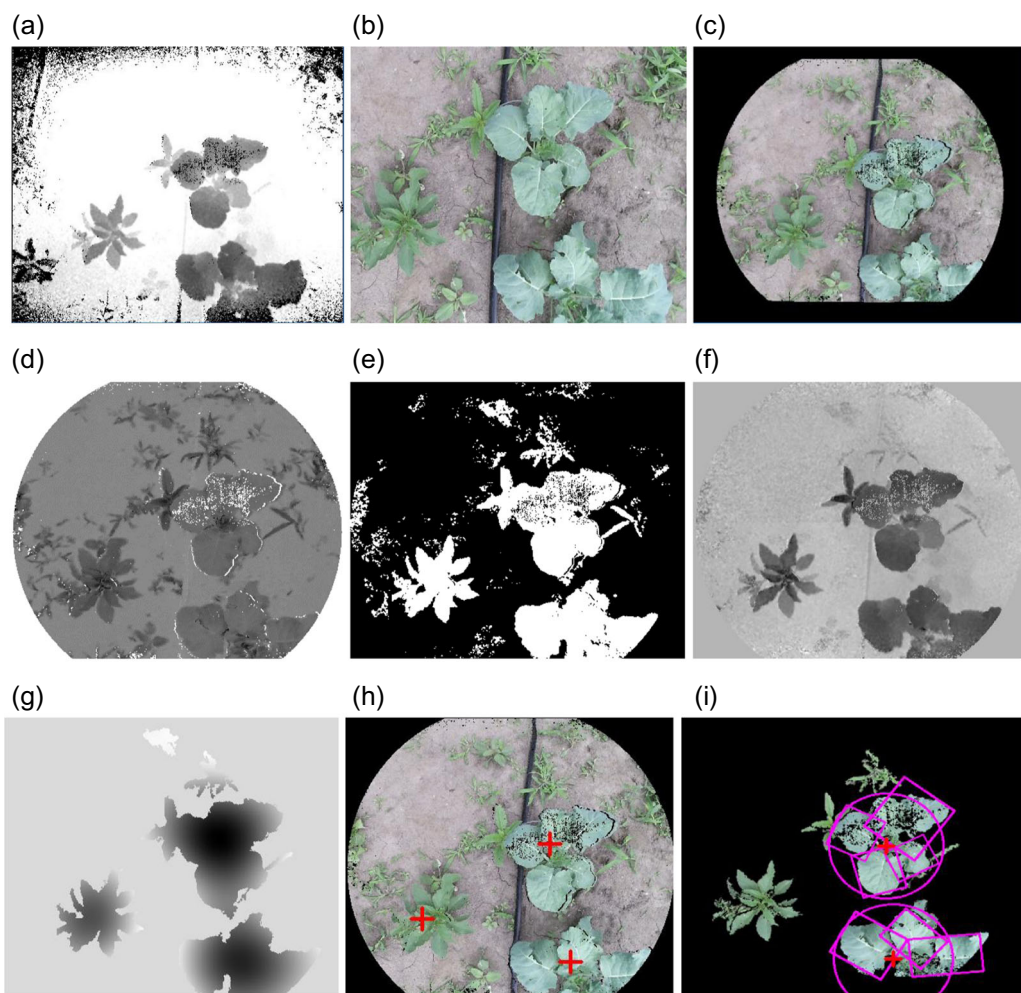


FIGURE 15 Sample broccoli plants images (16 DAT; 40 k lux) at each image processing step including: (a) depth and (b) color images; (c) color registration and filtered image; (d) color-based weight map for segmentation; (e) segmented image, with white vegetation pixels; (f) above-ground distance map; (g) masked amplitude map of wavelet transformation; (h) detected plants marked with crosses; and (i) feature-based localization refinement and classification with target crop plants labeled with crosses [Color figure can be viewed at wileyonlinelibrary.com]

broccoli 13 DAT, since the crop canopy shape was found nonspherical and nonisotropic. The results of plant detection and localization, and the result after feature-based refinement at different growth stages were listed and compared.

4.4 | Feature-based classification performance

The crop/noncrop classification performance (after Step 6) was evaluated using the minimized 10-fold CV classification error. In this study, broccoli 13 DAT were found having extractable leaves with substantial features useful for crop/noncrop classification, so the two-layer classification method described before was applied. In the classification of lettuce and broccoli less than 13 days, only canopy features were used, thus it is in a one-layer classification schema. Seven algorithms were applied to train models with the features extracted from the detected plants. During model tuning, about 10 preset values were selected for each parameter, and the models were examined with all parameter combinations to get the minimized CV errors. The overfitting problem was considered by monitoring both

training error and CV error during tuning. The best performance of each model was recorded and analyzed in terms of their 10-fold CV errors, and the training error.

5 | RESULTS AND DISCUSSION

5.1 | Segmentation performance and performance improvement verification

In the comparison experiments, with the depth-only segmentation algorithm, on average, 89.6% of the broccoli images and 74.2% of the lettuce images were segmented successfully ($\text{IoU} > 75\%$; Equation (10)). With the color-only segmentation algorithm, on average 77.4% of the broccoli images and 81.2% of the lettuce images were segmented successfully ($\text{IoU} > 75\%$). With the color-depth fusion-based segmentation algorithm, on average 96.6% of the broccoli images and 92.4% of the lettuce images were segmented with IoU greater than 75%. The results for different DAT's of different algorithms were listed in Table 1.

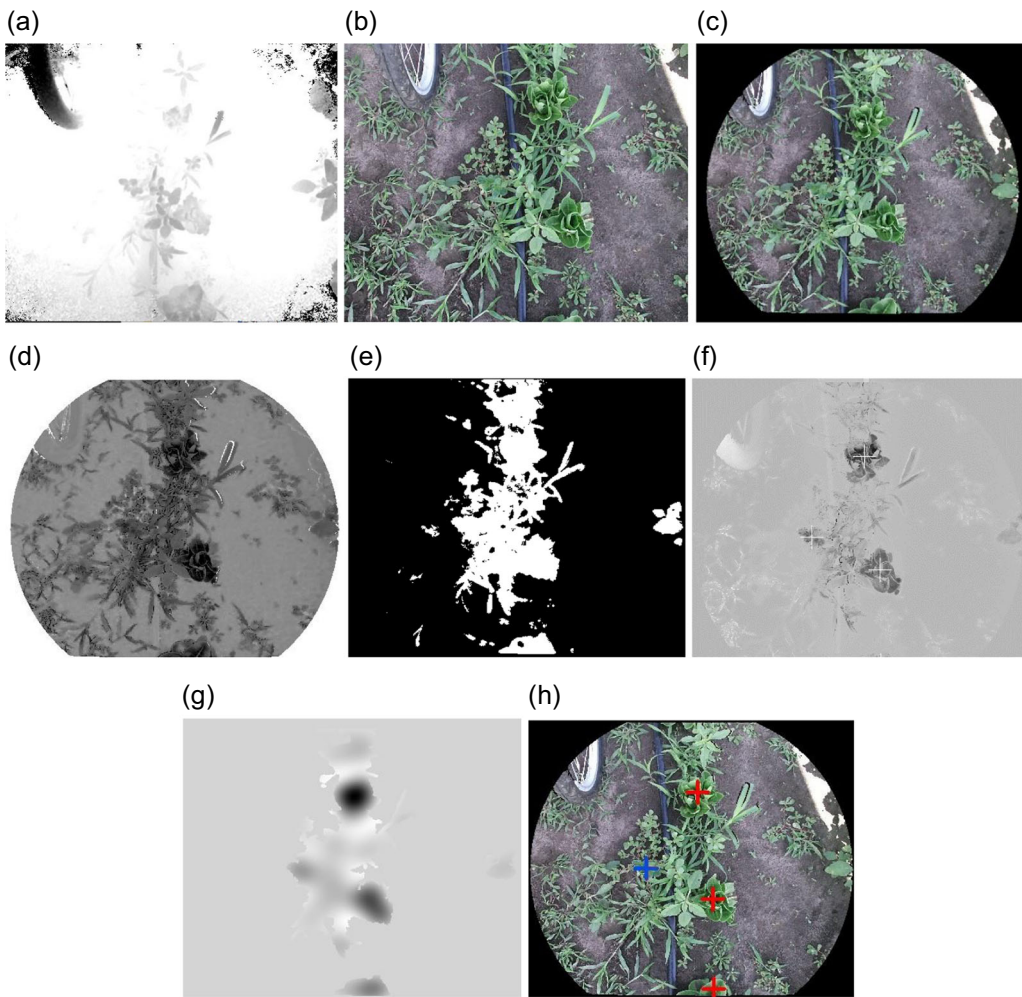


FIGURE 16 Sample lettuce plants images (taken at 22 DAT; 8 k lux). (a) Depth and (b) color images; (c) color registration and filtered image; (d) color-based weight map for segmentation; (e) segmented image, with white vegetation pixels; (f) above-ground distance map; (g) masked amplitude map of wavelet transformation; and (h) crop plants detection and localization results marked with red crosses [Color figure can be viewed at wileyonlinelibrary.com]

The fusion-based segmentation method showed higher segmentation performance in most tested situations than the color-based and depth-based algorithms with similar algorithm complexity.

The failures of the depth-based algorithm mainly occurred in two scenarios. When too many outlier points or vegetation pixels were present, then the soil surface was barely visible, the RANSAC algorithm detected planes with points from plant leaves. Lower segmentation performance was also observed when the crops plants were low in height and the soil surface was not even, especially at early growth stages with the existence of ridges in the soil. In such situation, the target crop plants were likely to be segmented as background. Representative failure cases of the depth-based method are shown in Figures 12 and 13.

Higher segmentation performance of the color-based method was observed in cloudy days, in which the ambient light intensity remained consistent in the image. In most failure cases, numerous vegetation pixels illuminated by the extreme high or low light

intensity were classified as background, which usually happened in sunny days. Representative failure cases of the color-based method are shown in Figure 14.

The color-depth fusion method was more robust than the depth-based or the color-based method alone except when plants were at quite early growth stages. Specifically, the fusion-based method was more robust to high weed density than the depth-based method (Figure 13c), and it is more robust to extreme lighting conditions than the color-based method (Figure 14c). However, in this study, the fusion-based method still yielded a lower success rate than the color-based method at early growth stages (broccoli DAT < 7; lettuce DAT < 12). That was because some crop plants were even lower than the variation in the soil surface, and even with the color weight, they were segmented as background. Thus, at early growth stages (broccoli DAT < 7; lettuce DAT < 12), color-based segmentation was a better choice, and the results of the color-based method were used for the following steps.

TABLE 2 The result of segmentation, plant extraction, and localization steps for broccoli and lettuce at different growth stages

	Days after transplanting	3-7	8-12	13-17	18-22	23-27	Average
	Estimated weed coverage (%)	5-10	5-15	15-30	25-45	35-50	
Broccoli	Segmentation success rate (%)	100	100	100	99.0	96.0	99.0
	Plant extraction recall (%)	100	100	96.3	74.1	67.5	87.6
	Feature-based refined extraction recall (%)	100	100	98.2	87.1	84.5	93.9
	Average crop plant localization error (MAE) ± standard deviation (mm)	10.2 ± 2.4	12.7 ± 2.2	14.1 ± 3.1	40.8 ± 9.7	52.6 ± 16.6	26.8 ± 6.8
Lettuce	Segmentation success rate (%)	100	100	100	98.0	90.0	97.6
	Plant extraction recall (%)	100	100	100	93.3	82.7	95.2
	Average crop plant localization error (MAE) ± SD (mm)	4.9 ± 1.5	5.2 ± 1.9	6.9 ± 2.0	9.4 ± 2.9	10.3 ± 3.5	7.4 ± 2.4

Additional examples of broccoli and lettuce segmentation results are shown in Figures 15 and 16 as step results of the entire image processing pipeline.

5.2 | Plant extraction and localization

Without feature-based refinement, on average 87.6% of the broccoli plants and 95.2% of the lettuce plants were correctly extracted (recall) at all growth stages. 69.1% and 87.4% of the detected plants were correct detections, which were actual broccoli or lettuce (precision).

For broccoli images collected greater than 13 DAT, the plant extraction results were refined. The overall recall of the broccoli plants extraction step was improved to 93.9%. The overall precision of the broccoli extraction step was improved to 84.4%.

The average localization errors (MAE) of the crop plant stems after feature-based refinement were 26.8 and 7.4 mm for broccoli and lettuce, respectively. The average standard deviation of the localization errors were 6.8 and 2.4 mm for broccoli and lettuce, respectively.

It was observed that the error of plant extraction and localization increased as the crop plants grows (Table 2). Examples of broccoli and lettuce extraction and localization runtime results are shown in Figures 15 and 16.

As an observation, before feature-based refinement, images with high weed densities or with large weed plants end up with larger localization error and larger misdetection rate. This result was due to wrong plant detection by the blob detection algorithm and localization results with affection from weeds connected to the crop plants and some large weed plants. After feature-based refinement, which was applied to the broccoli 13 DAT, the accuracy of broccoli plant extraction and localization both improved. But since the venation extraction algorithm relied on

TABLE 3 Model evaluation and comparison results of broccoli leaf classification

Model	Tuning parameters	Training error	CV error
LR	None	5.2%	8.6%
ANN	Layer = (5, 2)	5.1%	15.4%
KNN	K = 5	8.3%	11.3%
SVM	Kernel = radial Gamma = 0.01 Cost = 100	5.3%	10.7%
QDA	None	6.4%	9.5%
RandomForest	N = 500	13.8%	17.0%
AdaBoost	TreeDepth = 4 Iter = 100 Nu = 0.2	5.7%	7.3%

Note: Listed are the minimized training errors, and CV errors, with the corresponding tuning parameters.

Abbreviation: ANN, artificial neural network; KNN, k-nearest neighbors; LR, logistic regression; QDA, quadrature discriminant analysis; SVM, support vector machine.

TABLE 4 Model evaluation and comparison results of broccoli plant classification

Model	Tuning parameters	Training error	CV error
LR	None	7.2%	10.2%
ANN	Layer = (5, 2)	3.7%	11.9%
KNN	K = 3	10.5%	14.3%
SVM	Kernel = radial Gamma = 0.01 Cost = 100	3.6%	5.6%
QDA	None	4.4%	10.4%
RandomForest	N = 500	7.7%	8.4%
AdaBoost	TreeDepth = 4 Iter = 50 Nu = 0.1	2.6%	3.1%

Note: Listed are the minimized training errors, and CV errors, with the corresponding tuning parameters.

the color information, it was still observed to be vulnerable to the inconsistent illumination problems, such as image saturation and shadow effects.

5.3 | Classification

The feature extraction algorithm described in 3.4 was applied to the plant extraction results. In this study, for broccoli, 806 sets of canopy features 2,858 sets of leaf features were extracted. For lettuce, 718 sets of canopy features were extracted. In the following subsections, the results were presented separately for broccoli classification and lettuce classification.

TABLE 5 Model evaluation and comparison results of lettuce plant classification. Listed are the minimized training errors, and CV errors, with the corresponding tuning parameters

Model	Tuning parameters	Training error	CV error
LR	None	10.8%	13.4%
ANN	Layer = (5, 2)	8.3%	16.1%
KNN	K = 5	9.9%	14.2%
SVM	Kernel = polynomial Gamma = 0.05 Cost = 10	7.2%	9.0%
QDA	None	7.9%	10.5%
RandomForest	N = 500	8.4%	11.2%
AdaBoost	TreeDepth = 4 Iter = 50 Nu = 0.1	5.1%	6.8%

Note: Listed are the minimized training errors, and CV errors, with the corresponding tuning parameters.

Abbreviation: ANN, artificial neural network; KNN, k-nearest neighbors; LR, logistic regression; QDA, quadrature discriminant analysis; SVM, support vector machine.

5.3.1 | Broccoli classification

As mentioned above, broccoli classification has two stages. One stage is leaf/nonleaf classification using leaf features, and the other is crop/noncrop classification. The minimized CV errors of different methods in leaf/nonleaf classification are displayed in Table 3. In crop/noncrop classification, the canopy features as well as the classified crop plant leaf features of each separated plant were used. As a result, the lowest average error rate achieved in broccoli crop/noncrop classification was 3.1% during CV, with the false-positive rate of 1.1% and the false-negative rate of 2.0% (Table 4).

5.3.2 | Lettuce classification

Since only a few leaves can be extracted from the lettuce data set, the crop/noncrop classification was performed by using only canopy features of the separated plants. As a result, the lowest average error rate achieved in lettuce crop was 6.8% on average in CV, and with false-positive rate of 4.0% and false-negative rate of 2.8% (Table 5).

Most of the classifiers were performing well in both stages of crop/noncrop classification. Some nonlinear parametric classifiers such as AdaBoost and SVM have slightly better performance. Thus, it can be concluded that the extracted features can represent the differences between crop and noncrop plants well. Several reasons that these nonlinear classifiers performed better are as follows: (a) The features extracted in this study created a nonlinear decision boundary for examined plants. Crops are in the same patterns, and others are all noncrops. Linear models (LR and QDA) with sigmoid-shaped responses were not suitable because of the models' linear decision boundaries. (b) In this study, only about 10 predictors were used after dimension reduction. Thus, Random Forest, which is mainly used with many predictors available and to find the most valuable features, was less suitable than nonlinear SVM and AdaBoost. Further discussions about the failures about different classifiers will be studied in our further publications.

For the entire system, by combining the results of all the steps (plant extraction and feature-based classification), the system detected 91.7% of broccoli plants on average at all tested growth stages, and 1.1% of the detected broccoli plants were false-positive. The average broccoli localization error was 26.8 mm. The system detected 90.8% of the lettuce plants, and 4.0% of the detected lettuce plants were false-positive. The average lettuce localization error was 7.4 mm. The entire algorithm took about 300 ms for each image on a laptop with an Intel i7-4600 m CPU. The implication is that the proposed algorithm on a regular PC will support travel at about 2 mph to detect and localize broccoli and lettuce with reported accuracy for a robotic weeding application.

6 | CONCLUSIONS

In this paper, we proposed an image processing pipeline for detecting and localizing broccoli and lettuce crop plants by fusing color and depth images. For both crops (broccoli and lettuce) the detection

algorithms produced high true positive detection rates (91.7% and 90.8%, respectively) and low average false discovery rates (1.1% and 4.0%, respectively). The average localization errors of the crop plant stems were 26.8 and 7.4 mm for broccoli and lettuce, respectively. The fusion of color and depth improved the average crop plant segmentation success rates from 87.2% (depth-based) and 76.4% (color-based) to 96.6% for broccoli, and from 74.2% (depth-based) and 81.2% (color-based) to 92.4% for lettuce, respectively. The fusion-based algorithm had reduced performance in detecting crop plants at early growth stages. From the result of the experiments conducted, we can conclude that

- The fusion of color and depth is beneficial to the segmentation of plants from background with same algorithm complexity at most tested growth stages. However, the fusion is less effective than using color only at early growth stages (broccoli DAT < 7; lettuce DAT < 12).
- Enhanced by the fusion of both color images and depth images, the crop plant detection algorithm was capable of detecting and localizing broccoli and lettuce plants at different growth stages with high weed densities in the background of the images.

The framework of the proposed algorithm can be extended to different crop species, and the developed algorithm can be applicable to other applications such as selective spraying and plant mapping.

ACKNOWLEDGMENTS

The research is sponsored by Leopold Center for Sustainable Agriculture (Grants Nos. M2009-23 and M2012-24) and USDA NIFA Foundational Programs (Grant No. 20136702121126).

ORCID

Lie Tang  <http://orcid.org/0000-0002-8719-5378>

REFERENCES

- Andújar, D., Dorado, J., Fernández-Quintanilla, C., Ribeiro, A., Andújar, D., Dorado, J., & Ribeiro, A. (2016). An approach to the use of depth cameras for weed volume estimation. *Sensors*, 16(7), 972. <https://doi.org/10.3390/s16070972>
- Andújar, D., Weis, M., & Gerhards, R. (2012). An ultrasonic system for weed detection in cereal crops. *Sensors*, 12(12), 17343–17357. <https://doi.org/10.3390/s121217343>
- Bawden, O., Kulk, J., Russell, R., McCool, C., English, A., Dayoub, F., & Perez, T. (2017). Robot for weed species plant-specific management. *Journal of Field Robotics*, 34(6), 1179–1199. <https://doi.org/10.1002/rob.21727>
- Chen, Y. S., & Hsu, W. H. (1988). A modified fast parallel algorithm for thinning digital patterns. *Pattern Recognition Letters*, 7(2), 99–106. [https://doi.org/10.1016/0167-8655\(88\)90124-9](https://doi.org/10.1016/0167-8655(88)90124-9)
- Corti, A., Giancola, S., Mainetti, G., & Sala, R. (2016). A metrological characterization of the Kinect V2 time-of-flight camera. *Robotics and Autonomous Systems*, 75, 584–594. <https://doi.org/10.1016/j.robot.2015.09.024>
- Dyrmann, M., Jørgensen, R. N., & Midtiby, H. S. (2017). RoboWeedSupport – Detection of weed locations in leaf occluded cereal crops using a fully convolutional neural network. *Advances in Animal Biosciences*, 8(02), 842–847. <https://doi.org/10.1017/S2040470017000206>
- Dyrmann, M., Christiansen, P., & Midtiby, H. S. (2018). Estimation of plant species by classifying plants and leaves in combination. *Journal of Field Robotics*, 35(2), 202–212. <https://doi.org/10.1002/rob.21734>
- Dyrmann, M., Karstoft, H., & Midtiby, H. S. (2016). Plant species classification using deep convolutional neural network. *Biosystems Engineering*, 151, 72–80. <https://doi.org/10.1016/J.BIOSYSTEMSENG.2016.08.024>
- Fankhauser, P., Bloesch, M., Rodriguez, D., Kaestner, R., Hutter, M., & Siegwart, R. (2015). Kinect v2 for mobile robot navigation: Evaluation and modeling. *Advanced Robotics, ICAR 2015*, Kadir Has University, Istanbul, Turkey, pp. 388–394. <https://doi.org/10.1109/ICAR.2015.7251485>
- Finlayson, G. D., Hordley, S. D., & Drew, M. S. (2002). Removing shadows from images. *Computer Science*, 2353(1), 823–836. <https://doi.org/10.1109/TPAMI.2006.18>
- Foglia, M. M. M., & Reina, G. (2006). Agricultural robot for radicchio harvesting. *Journal of Field Robotics*, 23(6–7), 363–377. <https://doi.org/10.1002/rob.20131>
- Gai, J. (2016). *Plants detection, localization and discrimination using 3D machine vision for robotic intra-row weed control* (Graduate Theses and Dissertations). Iowa State University. 15703. <https://lib.dr.iastate.edu/etd/15703>
- Gerhards, R., & Christensen, S. (2003). Real-time weed detection, decision making and patch spraying in maize, sugarbeet, winter wheat and winter barley. *Weed Research*, 43(6), 385–392. <https://doi.org/10.1046/j.1365-3180.2003.00349.x>
- Hamuda, E., Mc Ginley, B., Glavin, M., & Jones, E. (2017). Automatic crop detection under field conditions using the HSV colour space and morphological operations. *Computers and Electronics in Agriculture*, 133, 97–107. <https://doi.org/10.1016/j.compag.2016.11.021>
- Herrera, C. D., Kannala, J., & Heikkila, J. (2012). Joint depth and color camera calibration with distortion correction. *IEEE Transactions on Pattern Analysis and Machine Intelligence*, 34(10), 2058–2064. <https://doi.org/10.1109/TPAMI.2012.125>
- Huang, G., Liu, Z., Van Der Maaten, L., & Weinberger, K. Q. (2017). Densely connected convolutional networks. Proceedings of 30th IEEE Conference on Computer Vision and Pattern Recognition, CVPR 2017, Honolulu, HI, January 2017, 2261–2269. <https://doi.org/10.1109/CVPR.2017.243>
- Jin, J., & Tang, L. (2009). Corn plant sensing using real-time stereo vision. *Journal of Field Robotics*, 26(6–7), 591–608. <https://doi.org/10.1002/rob.20293>
- Kamilaris, A., & Prenafeta-Boldú, F. X. (2018). Deep learning in agriculture: A survey. *Computers and Electronics in Agriculture*, 147, 70–90. <https://doi.org/10.1016/J.COMPAG.2018.02.016>
- Kise, M., Zhang, Q., & Rovira Más, F. (2005). A stereovision-based crop row detection method for tractor-automated guidance. *Biosystems Engineering*, 90(4), 357–367. <https://doi.org/10.1016/J.BIOSYSTEMSENG.2004.12.008>
- Kusumam, K., Krajník, T., Pearson, S., Duckett, T., & Cielniak, G. (2017). 3D-vision based detection, localization, and sizing of broccoli heads in the field. *Journal of Field Robotics*, 34(8), 1505–1518. <https://doi.org/10.1002/rob.21726>
- Li, J., & Tang, L. (2018). Crop recognition under weedy conditions based on 3D imaging for robotic weed control. *Journal of Field Robotics*, 35(4), 596–611. <https://doi.org/10.1002/rob.21763>
- Long, J., Shelhamer, E., & Darrell, T. (2015). Fully convolutional networks for semantic segmentation. Proceedings of the IEEE Conference on Computer Vision and Pattern Recognition, Boston, MA, 2015, 3431–3440.
- Lottes, P., Hörfelerin, M., Sander, S., & Stachniss, C. (2017). Effective vision-based classification for separating sugar beets and weeds for precision farming. *Journal of Field Robotics*, 34(6), 1160–1178. <https://doi.org/10.1002/rob.21675>

- Marcus, G. (2018). Deep learning: A critical appraisal. Retrieved from <https://arxiv.org/abs/1801.00631>
- McCool, C., Perez, T., & Upcroft, B. (2017). Mixtures of lightweight deep convolutional neural networks: Applied to agricultural robotics. *IEEE Robotics and Automation Letters*, 2(3), 1344–1351. <https://doi.org/10.1109/LRA.2017.2667039>
- Milioto, A., Lottes, P., & Stachniss, C. (2017). Real-time blob-wise sugar beets vs weeds classification for monitoring fields using convolutional neural networks. *ISPRS Annals of the Photogrammetry, Remote Sensing and Spatial Information Sciences*, 4(2W3), 41–48. <https://doi.org/10.5194/isprs-annals-IV-2-W3-41-2017>
- Nguyen, T. T., Vandaele, K., Wouters, N., Kayacan, E., De Baerdemaeker, J. G., & Saeys, W. (2016). Detection of red and bicoloured apples on tree with an RGB-D camera. *Biosystems Engineering*, 146, 33–44. <https://doi.org/10.1016/j.BIOSYSTEMSENG.2016.01.007>
- Pannacci, E., Lattanzi, B., & Tei, F. (2017). Non-chemical weed management strategies in minor crops: A review. *Crop Protection*, 96, 44–58. <https://doi.org/10.1016/j.croppro.2017.01.012>
- Philipp, I., & Rath, T. (2002). Improving plant discrimination in image processing by use of different colour space transformations. *Computers and Electronics in Agriculture*, 35(1), 1–15. [https://doi.org/10.1016/S0168-1699\(02\)00050-9](https://doi.org/10.1016/S0168-1699(02)00050-9)
- Piron, A., van der Heijden, F., & Destain, M. F. (2011). Weed detection in 3D images. *Precision Agriculture*, 12(5), 607–622. <https://doi.org/10.1007/s11119-010-9205-2>
- Potena, C., Nardi, D., & Pretto, A. (2017). Fast and accurate crop and weed identification with summarized train sets for precision agriculture. *Advances in Intelligent Systems and Computing*, 531, 105–121. https://doi.org/10.1007/978-3-319-48036-7_9
- Ruckelshausen, A., Biber, P., Dorna, M., Gremmes, H., Klose, R., & Linz, A., et al. (2009). BoniRob—An autonomous field robot platform for individual plant phenotyping. *Precision Agriculture*, 9(841), 1.
- Sa, I., Lehnert, C., English, A., McCool, C., Dayoub, F., Upcroft, B., & Perez, T. (2017). Peduncle detection of sweet pepper for autonomous crop harvesting—Combined color and 3-D information. *IEEE Robotics and Automation Letters*, 2(2), 765–772. <https://doi.org/10.1109/LRA.2017.2651952>
- dos Santos Ferreira, A., Matte Freitas, D., Gonçalves da Silva, G., Pistori, H., & Theophilo Folhes, M. (2017). Weed detection in soybean crops using ConvNets. *Computers and Electronics in Agriculture*, 143, 314–324. <https://doi.org/10.1016/j.compag.2017.10.027>
- Shafarenko, L., Petrou, M., & Kittler, J. (1997). Automatic watershed segmentation of randomly textured color images. *IEEE Transactions on Image Processing*, 6(11), 1530–1544. <https://doi.org/10.1109/83.641413>
- Slaughter, D. C., Giles, D. K., & Downey, D. (2008). Autonomous robotic weed control systems: A review. *Computers and Electronics in Agriculture*, 61(1), 63–78. <https://doi.org/10.1016/j.compag.2007.05.008>
- Szegedy, C., Liu, W., Jia, Y., Sermanet, P., Reed, S., Anguelov, D., & Rabinovich, A. (2014). Going deeper with convolutions. Retrieved from <http://arxiv.org/abs/1409.4842>
- Szegedy, C., Vanhoucke, V., Ioffe, S., Shlens, J., & Wojna, Z. (2015). Rethinking the inception architecture for computer vision. Retrieved from <http://arxiv.org/abs/1512.00567>
- Tang, L., & Tian, L. F. (2008). Plant identification in mosaicked crop row images for automatic emerged corn plant spacing measurement. *Transactions of the ASABE*, 51(6), 2181–2191. <https://doi.org/10.13031/2013.25381>
- Tang, L., Tian, L. F., & Steward, B. L. (2000). Color image segmentation with genetic algorithm for in-field weed sensing. *Transactions of the ASAE*, 43(4), 1019–1027. <https://doi.org/10.13031/2013.2970>
- Tang, L., Tian, L. F., & Steward, B. L. (2003). Classification of broadleaf and grass weeds using gabor wavelets and an artificial neural network. *Transactions of the ASAE*, 46(4), 1247. <https://doi.org/10.13031/2013.13944>
- Tillett, N. D., Hague, T., Grundy, A. C., & Dedousis, A. P. (2008). Mechanical within-row weed control for transplanted crops using computer vision. *Biosystems Engineering*, 99(2), 171–178. <https://doi.org/10.1016/j.biosystemseng.2007.09.026>
- Tippetts, B., Lee, D. J., Lillywhite, K., & Archibald, J. (2016). Review of stereo vision algorithms and their suitability for resource-limited systems. *Journal of Real-Time Image Processing*, 11(1), 5–25. <https://doi.org/10.1007/s11554-012-0313-2>
- Underwood, J. P., Calleija, M., Taylor, Z., Hung, C., Nieto, J., Fitch, R., & Sukkarieh, S. (2015). Real-time target detection and steerable spray for vegetable crops. In Proceedings of the International Conference on Robotics and Automation: Robotics in Agriculture Workshop, Seattle, WA, USA, 26–30.
- USDA. (2016, September). 2015 Certified Organic Survey. Retrieved from <https://downloads.usda.library.cornell.edu/usda-esmis/files/zg64tk92g/pr76f6075/4f16c5988/OrganicProduction-09-15-2016.pdf>
- USDA. (2017, September). 2016 Certified Organic Survey. Retrieved from http://usda.mannlib.cornell.edu/current/OrganicProduction/OrganicProduction-09-20-2017_correction.pdf
- Van Der Weide, R. Y., Bleeker, P. O., Achten, V. T. J. M., Lotz, L. A. P., Fogelberg, F., & Melander, B. (2008). Innovation in mechanical weed control in crop rows. *Weed Research*, 48, 215–224. <https://doi.org/10.1111/j.1365-3180.2008.00629.x>
- Weiss, U., & Biber, P. (2011). Plant detection and mapping for agricultural robots using a 3D LIDAR sensor. *Robotics and Autonomous Systems*, 59(5), 265–273. <https://doi.org/10.1016/j.robot.2011.02.011>
- Weiss, U., Biber, P., Laible, S., Bohlmann, K., & Zell, A. (2010). Plant species classification using a 3D LIDAR sensor and machine learning. Proceedings of 9th International Conference on Machine Learning and Applications, ICMLA 2010, Washington DC, 339–345.
- Wu, S. G., Bao, F. S., Xu, E. Y., Wang, Y.-X., Chang, Y.-F., & Xiang, Q.-L. (2007). A leaf recognition algorithm for plant classification using probabilistic neural network. ISSPIT 2007 - 2007 IEEE International Symposium on Signal Processing and Information Technology, Cairo, Egypt, 2007, 11–16.
- Xia, C., Hwang, Y., Lee, D. H., Lee, J., & Lee, M. C. (2015). Three-dimensional plant leaf mapping and segmentation using kinect camera. 2015 54th Annual Conference of the Society of Instrument and Control Engineers of Japan, SICE 2015, Hangzhou, China, 1207–1211.

How to cite this article: Gai J, Tang L, Steward BL. Automated crop plant detection based on the fusion of color and depth images for robotic weed control. *J Field Robotics*. 2020;37:35–52. <https://doi.org/10.1002/rob.21897>